Progress In Electromagnetics Research, Vol. 107, 47–61, 2010

DESIGN AND ANALYSIS OF A MAGNETIC-GEARED ELECTRONIC-CONTINUOUSLY VARIABLE TRANSMISSION SYSTEM USING FINITE ELEMENT METHOD

L. Jian and K. T. Chau

Department of Electrical and Electronic Engineering
The University of Hong Kong
Pokfulam Road, Hong Kong, China

Abstract—This paper proposes a new electronic-continuously variable transmission (E-CVT) system for power-split hybrid electric vehicles (HEVs). The key is to integrate two permanent magnet motor/generators (M/Gs) together with a coaxial magnetic gear (CMG). By designing the modulating ring of the CMG to be rotatable, this integrated machine can achieve both power splitting and mixing, and therefore, can seamlessly match the vehicle road load to the engine optimal operating region. With the one-side-in and one-side-out structure and the non-contact transmission of the CMG, all the drawbacks aroused by the mechanical gears and chain existing in the traditional E-CVT system can be overcome. Moreover, the proposed E-CVT system possesses the merits of small size and light weight, which are vitally important for extending the full-electric drive range of HEVs. The working principle and the design details are elaborated. By using the finite element method (FEM), the electromagnetic characteristics are analyzed.

1. INTRODUCTION

Limited by the unsatisfactory performance of battery technologies and the high cost of fuel cells, hybrid electric vehicles (HEVs) have been considered as the best choice to bridge the current situations and the demands for clean and energy-efficient transportation. According to the types of the power-train, HEVs can be generally classified as series HEVs, parallel HEVs and power-split HEVs, in which the power-split HEVs combine the benefits of both the parallel types and the

Received 28 June 2010, Accepted 23 July 2010, Scheduled 31 July 2010
Corresponding author: L. Jian (lnjian@eee.hku.hk).

series types, hence offering the merits of ultra low emissions and high fuel economy [1]. The electronic-continuously variable transmission (E-CVT) system is one of the core components for the power-split HEVs [2]. It was firstly adopted by Toyota Prius in 1997 [3]. Then, several derivatives such as the GM-Allison compound E-CVT, the Timken compound split E-CVT and the Renault compound split E-CVT were introduced [4].

Figure 1 depicts the basic architecture of the Toyota Prius E-CVT system. It mainly consists of a planetary gear set (including a sun gear, a planet carrier which holds several planet gears meshed with the sun gear, and a ring gear with inward-facing teeth that mesh with the planet gears), two electric motor/generators (M/Gs) and two power electronic inverters. The engine shaft is connected to the planet carrier, and the rotor shafts of the two M/Gs are attached to the sun gear and the ring gear, respectively. The ring gear is connected to the final driveline through a silent chain and a counter gear to drive the wheels. By controlling the switching modes of the inverters, multiple power flows among the engine, the M/Gs and the battery can be achieved. Thus, the E-CVT system can seamlessly match the vehicle road load to the engine optimal operating region. However, the reliance on mechanical gears (including the planetary gear set and the

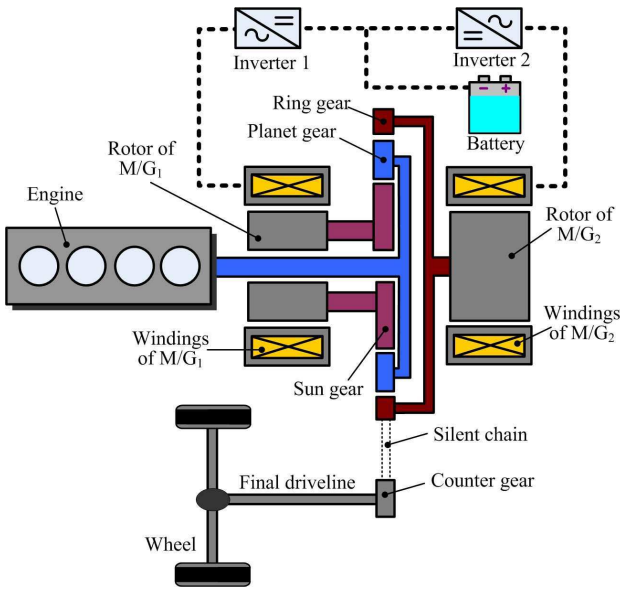

Figure 1. Toyota Prius E-CVT system.

counter gear) and the silent chain inevitably causes the drawbacks of transmission loss, gear noise and regular lubrication.

In order to get rid of the shortcomings arising form the contact mechanisms, the combination of two concentrically arranged machines were proposed to realize power splitting and mixing for HEVs [5, 6]. Unfortunately, slip rings and carbon brushes have to be equipped to inject/withdraw currents into/from the rotating armature windings. With no doubt, this will degrade the reliability of the whole system. Recently, a high performance coaxial magnetic gear (CMG) has been proposed [7, 8]. It can provide non-contact torque transmission and speed variation using the modulation effect of permanent magnet (PM) fields. Since all the PMs are involved to transmit torque, the CMG can offer as the torque density as high as its mechanical counterpart. Thus, it has promising industrial applications, such as EV drives [9] and wind power generation [10].

The purpose of this paper is to develop a new E-CVT system in which the CMG is adopted to supersede the mechanical planetary gear set. By integrating the two PM M/Gs together with the CMG, the one-side-in and one-side-out mechanical structure can be achieved so as to eliminate the silent chain and the counter gear employed in the traditional E-CVT system. Thus, the aforementioned drawbacks aroused by the mechanical planetary gear set can be overcome. Moreover, due to the high torque density of PM machines and the high extent of integration, the proposed E-CVT system possesses the merits of small size and light weight, which are vitally important for extending the full-electric drive range of HEVs. In Section 2, the system configuration and the operating principle will be introduced. Sections 3 and 4 will be devoted to the design of the integrated machine and its finite element analysis [11–14]. Finally, conclusion will be drawn in Section 5.

2. SYSTEM CONFIGURATION AND OPERATING PRINCIPLE

Figure 2 shows the configuration of the proposed E-CVT system. The key is to integrate the two M/Gs into a CMG which is shown in Fig. 3. PMs are mounted on both the inside and outside surfaces of the rotor of M/G_1, which also serves as the inner rotor of the CMG. Similarly, PMs are mounted on both the inside and outside surfaces of the rotor of M/G_2, which also serves as the outer rotor of the CMG. The stator of M/G_1 is deployed in the inner bore of the CMG and the stator of M/G_2 is located at the periphery of the CMG.

The engine shaft is connected to the modulating ring of the CMG,

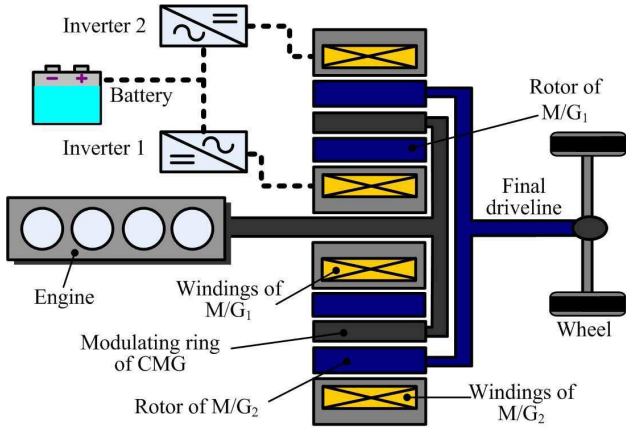

Figure 2. Proposed E-CVT system.

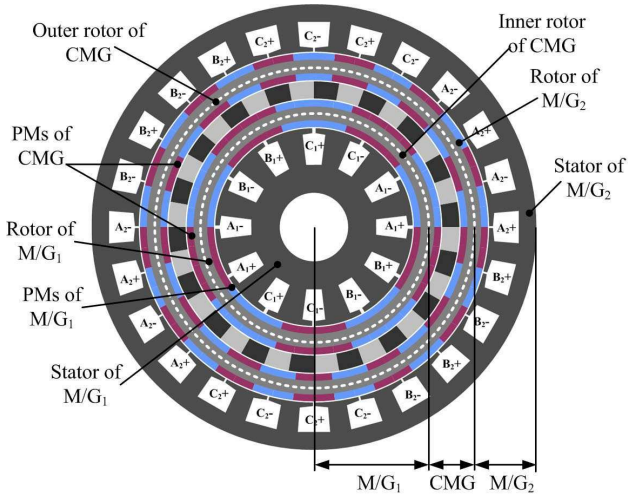

Figure 3. Integration of CMG and two M/Gs.

and the rotor shaft of the M/G_2 is attached to the final driveline. Therefore, it can offer multiple power flow paths as depicted in Fig. 4 to achieve power mixing or splitting. By adjusting the switching modes of the two inverters, the power flows can be controlled to offer: 1) seamless match between the vehicle road load and the engine optimal operating regime, therefore, resulting in a considerable reduction of the fuel consumption and greenhouse gas emission; 2) idle stop and

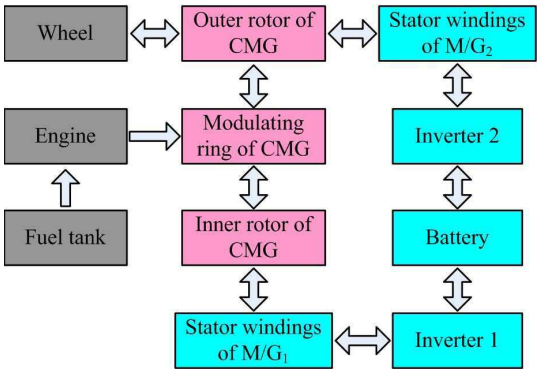

Figure 4. Power flow paths.

full electric launch, which can help save fuel when many stop-and-goes occur; 3) regenerative braking when the vehicle is slowing or coasting downhill. In addition, the drawbacks of transmission loss, gear noise and regular lubrication which are aroused from the mechanical contact mechanisms existing in the traditional E-CVT system can be totally eliminated by using non-contact magnetic gearing. Also, the high extent of integration can help improve the transmission efficiency and system reliability, as well as reduce the overall size and weight.

The working principle of the CMG lies on the magnetic field modulation of the modulating ring [15]. This modulating ring consists of several ferromagnetic segments which are symmetrically deployed in the airspace between its inner rotor and outer rotor. In order to enforce the structural strength, epoxy is filled in the air slots. By defining p_1 and p_2 as the pole-pair numbers of the inner and outer rotors of the CMG, respectively, and n_s as the number of ferromagnetic segments on the modulation ring, the CMG can achieve stable torque transmission when they satisfy the following relationship:

$$n_s = p_1 + p_2 \tag{1}$$

When the modulating ring is fabricated as a stationary component, the CMG can offer fixed-ratio variable speed transmission, and the corresponding speed relationship is given by:

$$\omega_1 = -\frac{p_2}{p_1}\omega_2 = -G_r\omega_2 \tag{2}$$

where ω_1, ω_2 are the rotational speeds of the outer rotor and inner rotor respectively, G_r is the so-called gear ratio, and the minus sign indicates that the two rotors rotate in opposite directions. In order to achieve multi-port power flow distribution, herein, the modulating

ring is purposely designed as another rotational component. The corresponding speed relationship is governed by:

$$\omega_1 + G_r\omega_2 - (1 + G_r)\omega_3 = 0 \tag{3}$$

where ω_3 is the rotational speed of the modulating ring. Without considering the power losses occurred in the CMG, it yields:

$$T_1\omega_1 + T_2\omega_2 + T_3\omega_3 = 0 \tag{4}$$

$$T_1 + T_2 + T_3 = 0 \tag{5}$$

where T_1, T_2 and T_3 are the developed magnetic torques on the inner rotor, the outer rotor and the modulating ring, respectively. Equations (3)–(5) demonstrate that when the modulating ring is designed to be rotatable, the CMG possesses similar functions as the planetary gear set [4], thus offering the capability of both power splitting and mixing which are the fundamentals of E-CVT system.

3. DESIGN OF THE INTEGRATED MACHINE

3.1. Determination of Gear Ratio and Power Specifications

The gear ratio G_r of the CMG and the power specifications of the two M/Gs are governed by the expected performance of the vehicle to be designed. Firstly, the distribution of the demanded working points of the final driveline can be determined by the driving cycle and the designed vehicle coefficients. Then the distribution of the demanded working points of each M/G can be deduced according to the fuel consumption map of the adopted engine and the energy management strategy [16] which will decide the power flows in the E-CVT system. Different gear ratios can deduce different power specifications of the M/Gs. Herein, $G_r = 2.6$ is adopted and the power specifications of the two M/Gs are listed in Table 1.

Table 1. Power specifications of M/Gs.

Rated power of M/G_1	15 kW
Rated speed of M/G_1	2500 rpm
Rated phase voltage of M/G_1	100 V
Rated power of M/G_2	30 kW
Rated speed of M/G_2	950 rpm
Rated phase voltage of M/G_2	100 V

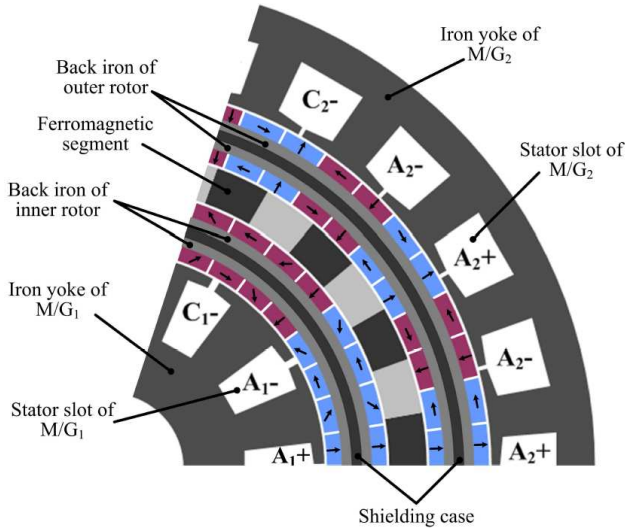

Figure 5. Construction of PM poles and rotors.

3.2. Construction of PM Poles and Rotors

The pole-pair numbers of the CMG are governed by (2). Hence, p_1 and p_2 equal to 5 and 13, respectively, are chosen to result in the gear ratio of 2.6. Consequently, n_s equals 18 can be deduced from (1). For this integrated machine, the decoupling of electromagnetic fields in the CMG and the two M/Gs is very important since it can directly affect the controllability of the system. Thus, the Halbach arrays are employed to constitute the PM poles on the two rotors. As shown in Fig. 5, each pole of PM is divided into 4 and 2 segments for the inner rotor and the outer rotor, respectively. The corresponding magnetization directions are indicated by the arrow lines. It is well known that, the Halbach arrays can offer the merit of self-shielding. Therefore, the back iron of the two rotors can be designed to have small thickness, leading to save iron material and reduce the system size. Moreover, non-magnetic shielding cases are sandwiched within the two rotors so as to offer further decoupling. The adoption of Halbach arrays can also help reduce the cogging torque and increase the torque transmission capability of the CMG [17].

3.3. Design of Stator Slots and Armature Windings

Fractional-slots and concentrated windings are adopted in the stators of the two M/Gs. The concentrated winding refers to the armature

winding that encircles a single stator tooth [18]. Fig. 6 illustrates the slots and winding connections on the stators of the two M/Gs. The numbers of slots are 12 and 24 on M/G_1 and M/G_2, respectively. Thus, the slot-per-phase-per-pole (SPP) of 2/5 and 8/13 are achieved for the M/G_1 and M/G_2, respectively.

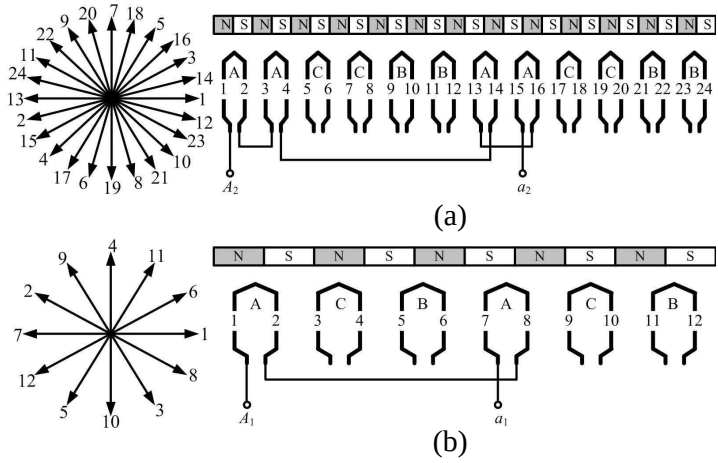

Figure 6. Slots and winding connections of two M/Gs. (a) M/G_1. (b) M/G_2.

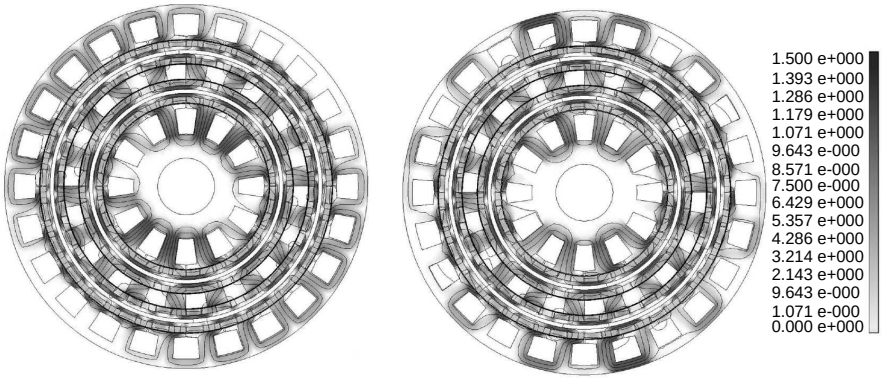

Figure 7. Electromagnetic field distributions in integrated machine: No load (left), Full load (right).

Table 2. Specifications of proposed machine.

No. of stator slots of M/G_1	12
No. of pole-pairs of M/G_1	5
No. of phases of M/G_1	3
No. of stator slots of M/G_2	24
No. of pole-pairs of M/G_2	13
No. of phases of M/G_2	3
No. of ferromagnetic segments	18
Length of airgaps	1 mm
Thickness of PMs	6 mm
Thickness of modulating ring	15 mm
Thickness of shielding cases	4 mm
Thickness of back iron of rotors	4 mm
Inside radius of stator of M/G_1	30 mm
Outside radius of stator of M/G_1	86.5 mm
Inside radius of stator of M/G_2	153.5 mm
Outside radius of stator of M/G_2	195 mm
Effective axial length	200 mm

4. FINITE ELEMENT ANALYSIS

The electromagnetic characteristics of the proposed integrated machine can be analyzed by using the finite element method (FEM). The specifications are listed in Table 2.

Firstly, the electromagnetic field distributions of the proposed machine under no-load and full-load are illustrated in Fig. 7. It can be observed that, almost no flux line goes through the shielding cases, which demonstrates that due to the adoptions of Halbach arrays and shielding cases, excellent field decoupling among the CMG and the two M/Gs can be achieved. With no doubt, this can help improve the controllability of the whole system. Therefore, the electromagnetic behavior of each component (namely the CMG and the two M/Gs) can be analyzed and modeled individually in spite of its integration.

Secondly, as shown in Fig. 8, the back electromotive force (EMF) waveforms can be obtained by rotating the two rotors of M/Gs at their rated speeds. Moreover, Fig. 9 gives their harmonic spectra. It can be found that, the harmonic contents existing in the two M/Gs are quite weak, which confirm that the Halbach array PMs can improve the distributions of magnetic fields.

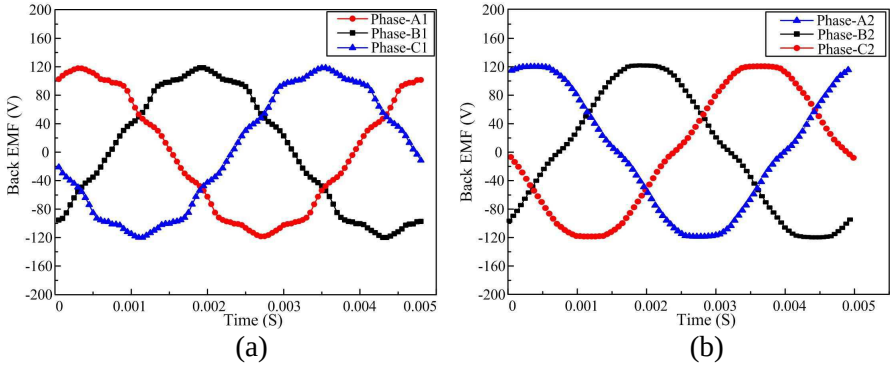

Figure 8. Back EMF waveforms at rated speeds. (a) M/G_1. (b) M/G_2.

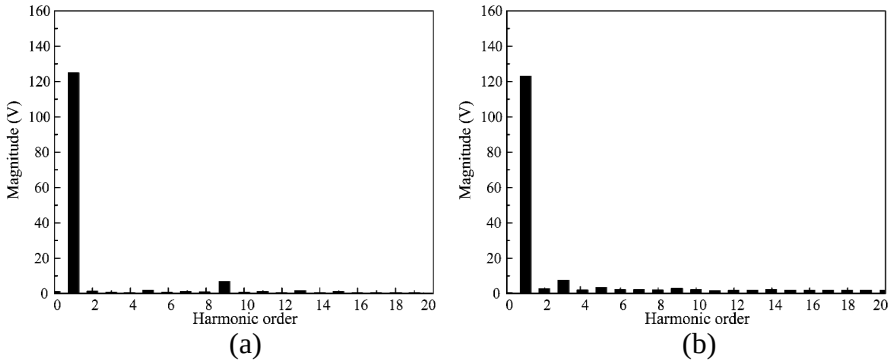

Figure 9. Harmonic spectra of back EMF at rated speeds. (a) M/G_1. (b) M/G_2.

Thirdly, the torque transmission capability of the CMG can be assessed by calculating the Maxwell's stress tensors in the airgaps while keeping the outer rotor and the modulating ring standstill, and rotating the inner rotor step by step. Fig. 10 depicts the resulting torque-angle curves. It can be found that, the torque-angle curves vary sinusoidally, in which the maximum torque values denote the pull-out torques. Thus, the pull-out torques of the inner rotor, outer rotor and modulating ring are 226.7 Nm, 589.7 Nm and 815.9 Nm, respectively. The ratio of the pull-out torques on the two rotors is 2.601, which has a very good agreement with the designed gear ratio of 2.6. In addition, the above three pull-out torques agree well with (5) since there is a phase difference of between the curve of the modulating ring and the curves of the two rotors.

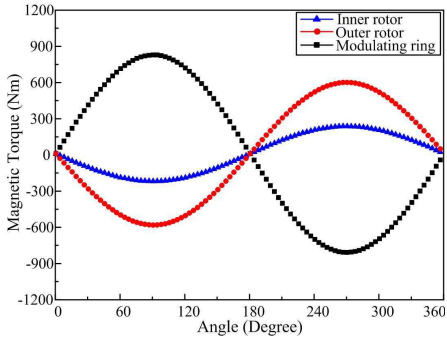

Figure 10. Torque-angle curves of CMG.

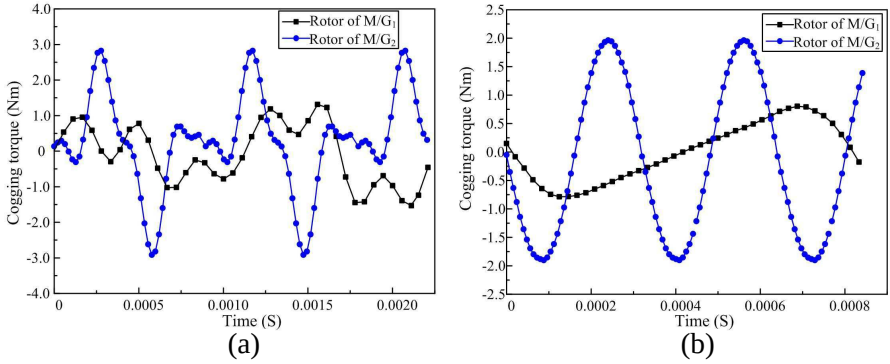

Figure 11. Cogging torques. (a) Caused by modulating ring. (b) Caused by stator slots.

Table 3. Parameters of two M/Gs.

	M/G_1	M/G_2
PM flux linkage ψ_{pm} [Wb]	0.094	0.108
Series turns per coil	12	9
Stator resistance [Ω]	0.084	0.080
d-axis inductances L_d [mH]	0.81	0.69
q-axis inductances L_q [mH]	0.81	0.69

Fourthly, the cogging torques can also be calculated using the Maxwell's stress tensors. By keeping the two rotors standstill and rotating the modulating ring, the cogging torques aroused by the air-slots of the modulating ring are obtained as shown in Fig. 11(a). Then,

by rotating the two rotors and the modulating ring simultaneously, the cogging torques aroused by the slots of the stators are obtained as shown in Fig. 11(b).

Finally, several important parameters can be calculated as listed in Table 3. Since non-salient PM poles are adopted in the two M/Gs, their d-axis inductances L_d are almost the same with the q-axis inductances L_q. Fig. 12 shows both the current and voltage constraints for operation of the M/Gs. The radius of the current limit circle R_I equals the rated current I_{rated}, while the radius of the voltage limit circle R_U is proportional to the voltage limit U_{lim} and inversely proportional to the rotational speed ω_r,. The stator current is has to

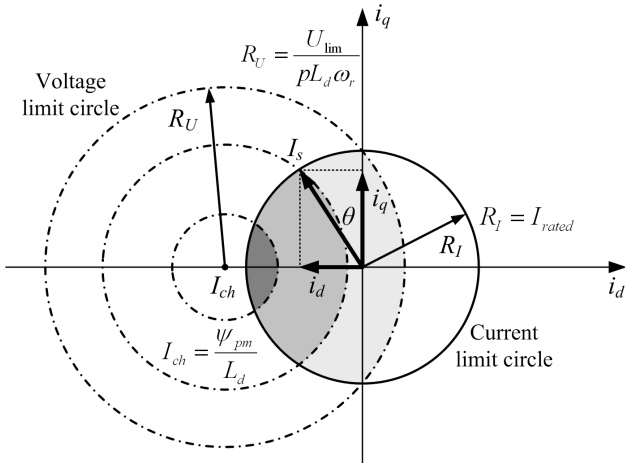

Figure 12. Current and voltage constraints for operation of M/Gs.

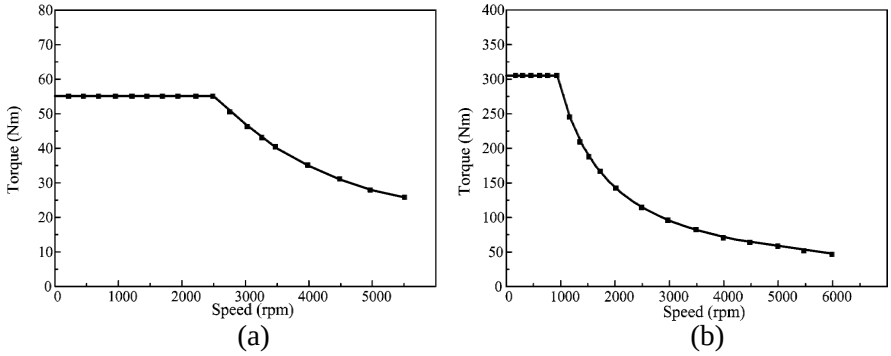

Figure 13. Torque-speed capabilities. (a) M/G_1. (b) M/G_2.

be located in the overlapping area of both the voltage and current limit circles. When the rotational speed is lower than the base speed, the stator current can be aligned along the q-axis to offer the maximum torque/current operation, namely the constant-torque operation. Once the rotational speed exceeds the base speed, the stator current has to divert away from the q-axis, and the corresponding id will weaken the stator flux linkage to ensure that the back EMF is lower than the voltage limit, namely the flux-weakening operation [19]. Fig. 13 shows the resulting torque-speed capabilities of the two M/Gs.

5. CONCLUSION

In this paper, a new E-CVT system for power-split HEVs has been designed and analyzed by using FEM. The key is to integrate two PM M/Gs together with a CMG. First, by purposely designing the modulating ring of the CMG to be rotatable, this integrated machine can achieve both power splitting and mixing, and therefore can seamlessly match the vehicle road load to the engine optimal operating region. Then, with the one-side-in and one-side-out structure and the non-contact transmission of the CMG, all the drawbacks aroused by the mechanical gears and chain existing in the traditional E-CVT system can be overcome. Finally, the proposed E-CVT system possesses the merits of small size and light weight, which are vitally important for extending the full-electric drive range of HEVs.

ACKNOWLEDGMENT

This work was supported by a grant (Project No. HKU7105/07E) from the Research Grants Council, Hong Kong Special Administrative Region, China.

REFERENCES

1. Chan, C. C. and K. T. Chau, *Modern Electric Vehicle Technology*, Oxford University Press, Oxford, 2001.
2. Chau, K. T. and C. C. Chan, "Emerging energy-efficient technologies for hybrid electric vehicles," *Proceedings of the IEEE*, Vol. 95, No. 4, 821–835, 2007.
3. Sasaki, S., "Toyota's newly developed hybrid powertrain," *IEEE International Symposium on Power Semiconductor Devices and ICs*, 17–22, 1997.

4. Miller, J. M., "Hybrid electric vehicle propulsion system architectures of the e-CVT type," *IEEE Trans. on Power Electron.*, Vol. 21, No. 3, 756–767, 2006.
5. Hoeijmakers, M. J. and J. A. Ferreira, "The electric variable transmission," *IEEE Trans. Ind. Appl.*, Vol. 42, No. 4, 1092–1100, 2006.
6. Eriksson, S. and C. Sadarangani, "A four-quadrant HEV drive system," *IEEE Vehicular Technology Conference*, 1510–1514, 2002.
7. Atallah, K., S. Calverley, and D. Howe, "Design, analysis and realization of a high-performance magnetic gear," *IEE Proc. Electric Power Appl.*, Vol. 151, No. 2, 135–143, 2004.
8. Jian, L. and K. T. Chau, "Analytical calculation of magnetic field distribution in coaxial magnetic gears," *Progress In Eletromagnetics Research*, Vol. 92, 1–16, 2009.
9. Chau, K. T., D. Zhang, J. Z. Jiang, C. Liu, and Y. Zhang, "Design of a magnetic-geared outer-rotor permanent-magnet brushless motor for electric vehicles," *IEEE Trans. Mag.*, Vol. 43, No. 6, 2504–2506, 2007.
10. Jian, L., K. T. Chau, and J. Z. Jiang, "A magnetic-geared outer-rotor permanent-magnet brushless machine for wind power generation," *IEEE Trans. Ind. Appli.*, Vol. 45, No. 3, 954–962, 2009.
11. Faiz, J. and B. M. Ebrahimi, "Mixed fault diagnosis in three-phase squirrel-cage induction motor using analysis of air-gap magnetic field," *Progress In Eletromagnetics Research*, Vol. 64, 239–255, 2006.
12. Vaseghi, B., N. Takorabet, and F. Meibody-Tabar, "Transient finite element analysis of induction machines with stator winding turn fault," *Progress In Eletromagnetics Research*, Vol. 95, 1–18, 2009.
13. Faiz, J., B. M. Ebrahimi, and M. B. B. Sharifian, "Time stepping finite element analysis of broken bars fault in a three-phase squirrel-cage induction motor," *Progress In Eletromagnetics Research*, Vol. 68, 53–70, 2007.
14. Chari, M., G. Bedrosian, J. D'Angelo, A. Konrad, G. Cotzas, and M. Shah, "Electromagnetic field analysis for electrical machine design," *Progress In Eletromagnetics Research*, Vol. 04, 159–211, 1991.
15. Jian, L. and K. T. Chau, "A coaxial magnetic gear with Halbach permanent magnet arrays," *IEEE Trans. Energy Conv.*, Vol. 25,

No. 2, 319–328, 2010.

16. Liu, J. and H. Peng, "Modeling and control of a power-split hybrid vehicle," *IEEE Trans. Control System Technol.*, Vol. 57, No. 1, 1242–1251, 2008.
17. Jian, L., K. T. Chau, Y. Gong, J. Z. Jiang, C. Yu, and W. Li, "Comparison of coaxial magnetic gears with different topologies," *IEEE Trans. Magn.*, Vol. 45, No. 10, 4526–4529, 2009.
18. EL-Refaie, A. M., "Fractional-slot concentrated-windings synchronous permanent magnet machines: Opportunities and challenges," *IEEE Trans. Ind. Electron.*, Vol. 57, No. 1, 107–121, 2010.
19. Sun, Z., J. Wang, G. Jewell, and D. Howe, "Enhanced optimal torque control of fault-tolerant PM machine under flux-weakening operation," *IEEE Trans. Ind. Electron.*, Vol. 57, No. 1, 344–353, 2010.